A low-mass dark matter search using ionization signals in XENON100

E. Aprile,[1] J. Aalbers,[2] F. Agostini,[3, 4] M. Alfonsi,[5] F. D. Amaro,[6] M. Anthony,[1] F. Arneodo,[7] P. Barrow,[8]
L. Baudis,[8] B. Bauermeister,[5, 9] M. L. Benabderrahmane,[7] T. Berger,[10] P. A. Breur,[2] A. Breskin,[11] A. Brown,[2]
E. Brown,[10] S. Bruenner,[12] G. Bruno,[13, 3] R. Budnik,[11, *] A. Buss,[13] L. Bütikofer,[14] J. M. R. Cardoso,[6]
M. Cervantes,[15] D. Cichon,[12] D. Coderre,[14] A. P. Colijn,[2] J. Conrad,[9, †] J. P. Cussonneau,[16] M. P. Decowski,[2]
P. de Perio,[1] P. Di Gangi,[4] A. Di Giovanni,[7] E. Duchovni,[11] A. D. Ferella,[3, 9] A. Fieguth,[13] D. Franco,[8]
W. Fulgione,[3, 17] M. Galloway,[8] M. Garbini,[4] C. Geis,[5] L. W. Goetzke,[1] Z. Greene,[1] C. Grignon,[5] E. Gross,[11]
C. Hasterok,[12] E. Hogenbirk,[2] R. Itay,[11] B. Kaminsky,[14] G. Kessler,[8] A. Kish,[8] H. Landsman,[11] R. F. Lang,[15]
L. Levinson,[11] M. Le Calloch,[16] C. Levy,[10] F. Linde,[2] S. Lindemann,[12] M. Lindner,[12] J. A. M. Lopes,[6]
A. Lyashenko,[18] A. Manfredini,[11] T. Marrodán Undagoitia,[12] J. Masbou,[16] F. V. Massoli,[4] D. Masson,[15] D. Mayani,[8]
A. J. Melgarejo Fernandez,[1] Y. Meng,[18] M. Messina,[1] K. Micheneau,[16] B. Miguez,[17] A. Molinario,[3] M. Murra,[13]
J. Naganoma,[19] U. Oberlack,[5] S. E. A. Orrigo,[6, ‡] P. Pakarha,[8] B. Pelssers,[9] R. Persiani,[16] F. Piastra,[8] J. Pienaar,[15]
G. Plante,[1] N. Priel,[11] L. Rauch,[12] S. Reichard,[15] C. Reuter,[15] A. Rizzo,[1] S. Rosendahl,[13] N. Rupp,[12] J. M. F. dos
Santos,[6] G. Sartorelli,[4] M. Scheibelhut,[5] S. Schindler,[5] J. Schreiner,[12] M. Schumann,[14] L. Scotto Lavina,[16]
M. Selvi,[4] P. Shagin,[19] H. Simgen,[12] A. Stein,[18] D. Thers,[16] A. Tiseni,[2, §] G. Trinchero,[17] C. D. Tunnell,[2, ¶]
M. von Sivers,[14] R. Wall,[19] H. Wang,[18] M. Weber,[1] Y. Wei,[8] C. Weinheimer,[13] J. Wulf,[8] and Y. Zhang[1]

(XENON Collaboration)

[1]*Physics Department, Columbia University, New York, NY, USA*
[2]*Nikhef and the University of Amsterdam, Science Park, Amsterdam, Netherlands*
[3]*INFN-Laboratori Nazionali del Gran Sasso and Gran Sasso Science Institute, L'Aquila, Italy*
[4]*Department of Physics and Astrophysics, University of Bologna and INFN-Bologna, Bologna, Italy*
[5]*Institut für Physik & Exzellenzcluster PRISMA, Johannes Gutenberg-Universität Mainz, Mainz, Germany*
[6]*Department of Physics, University of Coimbra, Coimbra, Portugal*
[7]*New York University Abu Dhabi, Abu Dhabi, United Arab Emirates*
[8]*Physik-Institut, University of Zurich, Zurich, Switzerland*
[9]*Department of Physics, Stockholm University, Stockholm, Sweden*
[10]*Department of Physics, Applied Physics and Astronomy, Rensselaer Polytechnic Institute, Troy, NY, USA*
[11]*Department of Particle Physics and Astrophysics, Weizmann Institute of Science, Rehovot, Israel*
[12]*Max-Planck-Institut für Kernphysik, Heidelberg, Germany*
[13]*Institut für Kernphysik, Wilhelms-Universität Münster, Münster, Germany*
[14]*Albert Einstein Center for Fundamental Physics, University of Bern, Bern, Switzerland*
[15]*Department of Physics and Astronomy, Purdue University, West Lafayette, IN, USA*
[16]*SUBATECH, Ecole des Mines de Nantes, CNRS/In2p3, Université de Nantes, Nantes, France*
[17]*INFN-Torino and Osservatorio Astrofisico di Torino, Torino, Italy*
[18]*Physics & Astronomy Department, University of California, Los Angeles, CA, USA*
[19]*Department of Physics and Astronomy, Rice University, Houston, TX, USA*
(Dated: June 16, 2016)

We perform a low-mass dark matter search using an exposure of $30\,\text{kg}\times\text{yr}$ with the XENON100 detector. By dropping the requirement of a scintillation signal and using only the ionization signal to determine the interaction energy, we lowered the energy threshold for detection to $0.7\,\text{keV}$ for nuclear recoils. No dark matter detection can be claimed because a complete background model cannot be constructed without a primary scintillation signal. Instead, we compute an upper limit on the WIMP-nucleon scattering cross section under the assumption that every event passing our selection criteria could be a signal event. Using an energy interval from $0.7\,\text{keV}$ to $9.1\,\text{keV}$, we derive a limit on the spin-independent WIMP-nucleon cross section that excludes WIMPs with a mass of $6\,\text{GeV}/c^2$ above $1.2 \times 10^{-41}\,\text{cm}^2$ at 90% confidence level.

---

* ran.budnik@weizmann.ac.il
† Wallenberg Academy Fellow
‡ Present address: IFIC, CSIC-Universidad de Valencia, Valencia,
  Spain
§ atiseni@nikhef.nl
¶ ctunnell@nikhef.nl

I. INTRODUCTION

Astrophysical observations indicate that dark matter (DM) is needed to explain structures ranging from the scales of galaxies to the largest observed scales [1]. Nevertheless, little is known about its nature. One theoretically favored candidate is a Weakly Interacting Massive Particle (WIMP). These particles may be detectable with experiments sensitive to WIMP-induced nuclear recoils [2].

Most WIMP models predict particles with a mass at the electroweak scale of $\sim 100\,\mathrm{GeV}/c^2$ [3]. However, there is also interest in light-mass DM, below $10\,\mathrm{GeV}/c^2$, prompted by *e.g.*, asymmetric models [4, 5] and claims of DM observations [6, 7]. Light-mass DM would yield low-energy events that are close to the experimental energy threshold of liquid-xenon detectors. Therefore, exploiting an approach that lowers the threshold [8], we investigate the spin-independent WIMP-nucleon cross section versus mass parameter space extending the XENON100 results for masses below $\sim 7.4\,\mathrm{GeV}/c^2$.

II. THE XENON100 DETECTOR

The XENON100 detector [9] is a dual-phase (liquid-gas) xenon Time Projection Chamber (TPC) located in the Laboratori Nazionali del Gran Sasso (LNGS). The TPC detection principle allows for measurements of nuclear recoils (NR) and electronic recoils (ER) through two signals: a prompt scintillation signal S1 and an ionization signal S2. The S1 signal is scintillation light from the rapid de-excitation of excited liquid xenon molecular states after an ionizing particle deposits energy. This deposition also liberates electrons, which drift in an electric field of $530\,\mathrm{V/cm}$ toward the liquid-gas interface, where a larger field of $\sim 12\,\mathrm{kV/cm}$ extracts them from the liquid. These accelerated electrons generate proportional scintillation in the xenon gas above the liquid.

Two arrays of 178 1"-square Hamamatsu R8520-AL PMTs are installed above and below the 62-kg xenon target. They detect both signals from the target. The distribution of the S2 signal among the top PMTs gives the projection of the interaction position on the PMT plane, while the relative time between the S1 and S2 signals provides the depth of the interaction, or z-coordinate. We distinguish ER and NR by the ratio of their respective S1 and S2 signals. A trigger identifies S2 signals, and the waveform of each PMT is digitized in the interval between $200\,\mu s$ before and after the trigger. The time for an electron to drift from the cathode to anode, or the maximum drift time, is $176\,\mu s$ [9]. The TPC is surrounded by an active veto region consisting of $99\,\mathrm{kg}$ of liquid xenon, instrumented with 64 PMTs optically isolated from the TPC.

In previous XENON100 analyses [10, 11], the recoil energy has been determined using the size of the S1 signal and the relative scintillation efficiency for the nuclear re-coils, $\mathcal{L}_{\mathrm{eff}}$, relative to the $122\,\mathrm{keV}$ calibration γ line of $^{57}\mathrm{Co}$ [10]. WIMPs with a mass below $10\,\mathrm{GeV}/c^2$ create NRs only up to a few keV, resulting in an S2 signal lower than a few hundred photoelectrons (PE) and an S1 signal that is often not detectable. Therefore for this analysis we only use the S2 signal to infer the energy.

III. ANALYSIS

This analysis is performed using the data from XENON100's Science Run II, which collected a 225 live-day exposure between February 28th, 2011 and March 31st, 2012 [10]. For the WIMP analysis, we drop the requirement of observing an S1 signal. This allows us to lower the effective threshold at the cost of losing z-coordinate reconstruction from the S2-S1 peaks time difference and particle identification based on the S2/S1 signal ratio. We perform a background-limited analysis on this previously unblinded dataset.

Both a NR and ER within liquid xenon will produce an S2 signal. We use calibration data of ERs and NRs taken with external $^{60}\mathrm{Co}/^{232}\mathrm{Th}$ and $^{241}\mathrm{AmBe}$ calibration sources, respectively. In these calibrations, photo-ionization and delayed extraction of electrons produce signals that have a mean size of $20\,\mathrm{PE}$ per electron [12]. We restrict ourselves to charge signal above $80\,\mathrm{PE}$, where the trigger efficiency is still at 80%, to minimize the background from these electrons. For the same reason, this value will be used as the lower threshold for the WIMP analysis.

For calibration events, to ensure that we only select valid low-energy events and to avoid a bias from few-electron background signals, we additionally require that the S1 signal observed in the TPC (at any size) has a co-incident S1 signal in the veto region. In this way, we create a low-energy recoil sample while still knowing that a scatter took place. These samples are then used to model the probability that a WIMP would pass our selection criteria (the WIMP acceptance). The acceptance loss for each condition, which will be described in this section, is determined using the fraction of events removed by this individual selection condition [13].

Many processes besides WIMP interactions can create S2 or S2-like signals in our detector, *e.g.*, radioactive backgrounds or photo-ionization of impurities or metallic surfaces in the TPC [12]. We use selection criteria to suppress these backgrounds. To begin, WIMPs are expected to interact uniformly in the liquid xenon target. In the DM search data, the event rate increases towards the radial edges of the detector. Therefore, we require that the reconstructed radius of the event is less than $13.4\,\mathrm{cm}$, which is approximately $2\,\mathrm{cm}$ from the TPC walls. This cut removes events from external backgrounds, which are stopped predominantly in the outer layers of the liquid target. The remaining liquid xenon target mass is $48.3\,\mathrm{kg}$. Within this target, the events are radially uniformly distributed, which means that a smaller fiducial
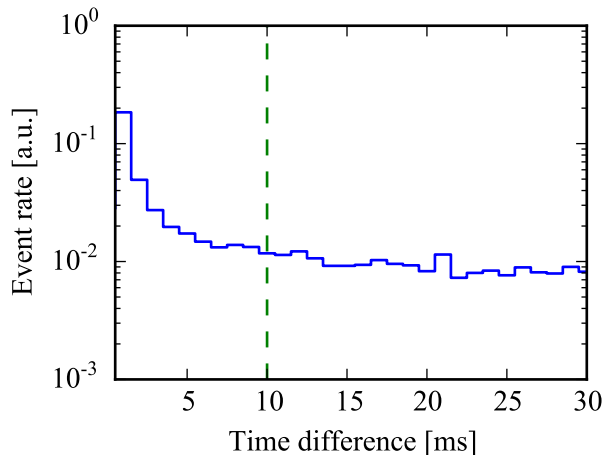
FIG. 1. Rate of events (S2 > 80 PE) as a function of the time difference from the previous recorded event. A cut is set at 10 ms to remove a population of events of small S2 signals (e.g., photo-ionization) that appears within a few ms from the previous trigger.

FIG. 2. S2 asymmetry parameter for ^{241}AmBe calibration data and a population of events produced in the xenon gas phase. We select interactions in the gas by requiring an S1 signal, small drift time, and a large S2 width using ^{60}Co and DM search data. An S2 asymmetry cut set at 0.17 is used to reject the gas event population.

volume does not reduce the background density.

Given an event with an S1 signal, we can use the information from that signal to isolate nuclear recoils using two additional cuts. First, the Monte Carlo nuclear-recoil model of [14] is used to determine a cut on the S1 size relative to the S2 size for any WIMP mass less than $20 \, \mathrm{GeV}/c^2$. We parametrize this Monte Carlo model by requiring that a nuclear recoil has – if present – an S1 signal less than $[4.7 + 0.012 \times (\mathrm{S2} - 80)] \, \mathrm{PE}$. This cut has an acceptance of 99.9% determined from the same Monte Carlo. Second, we can estimate the z-position of the interaction from the drift time between the S1 and S2 signals. We require the z-position to be more than 1.9 cm below the liquid-gas interface and more than 0.5 cm above the cathode. This condition decreases the fiducial volume by 8% and we conservatively assume an acceptance of 92% also for events without a detected S1 signal.

Secondary S2 signals can create events in which the main S2 signal is preceded or followed by similar nearby signals in the same event. These can be caused by multiple scatters in the active volume (i.e., not WIMPs) or misidentified detector artifacts. Additionally, any interaction in XENON100 can cause small S2 signals appearing up to milliseconds after the trigger, which are partly caused by photo-ionization on metal surfaces or impurities and possibly by delayed charge extraction as well [12]. We apply three cuts to remove these events.

First, events which contain too much baseline activity cannot be evaluated properly and are removed by comparing the area of the main S2 peak to the remaining baseline area. An S2 size-dependent threshold was derived using ^{241}AmBe calibration data and leads to a 94% WIMP acceptance. ER calibration data regularly acquired during the dark-matter run was used to monitor

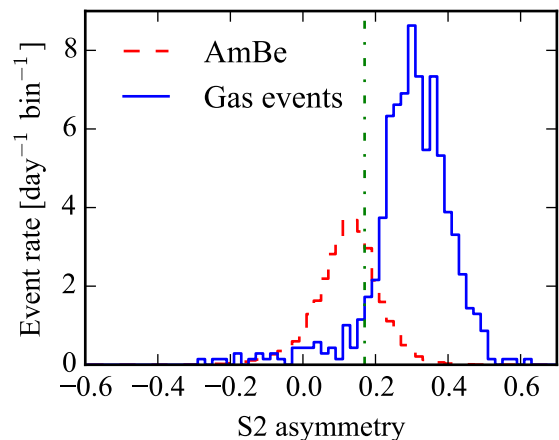the stability of the cut over time.

Second, we remove events which occur less than 10 ms after any other recorded event, resulting in a 2% livetime reduction. Figure 1 shows the event rate as a function of the time difference from the previous event. Signals caused by photo-ionization or delayed extraction are observed within a few ms from the previous event and are removed by this selection.

Third, we reject events with more than one S2 signal in the same event, e.g., multiple scatter events. If an S2 signal larger than 10 (30) PE is seen 176 μs before (after) the main S2 signal, the event is removed. The threshold after the main S2 signal is less strict since even a 250 PE S2 signal will itself create a secondary single-electron S2 signal ($\approx 20 \, \mathrm{PE}$ [12]) by photo-ionization in 10% of the cases. The acceptance loss is 3% at S2 = 100 PE and slowly increasing for larger S2 signals, as estimated by a model of induced S2 signals similar to [12], but extended to low-energies using the 10 ms time difference cut.

TABLE I. Acceptances of the different data selections and number of DM candidate events passing the selections. The cuts are applied sequentially. The number of events is in the S2 energy range [80, 1000] PE.

Description of cut	Acceptance at S2=100 PE	Events
Radial cut (starting events)	100%	537398
Depth and electronic recoil	92%	103914
Detector noise	94%	57516
Single S2 and 10 ms cut	95%	49041
Interaction in the gas	65%	13560

Finally, we apply a cut to remove events where the S2 signal is produced by an interaction in the gas between the anode and the top PMT screening electrode [9].
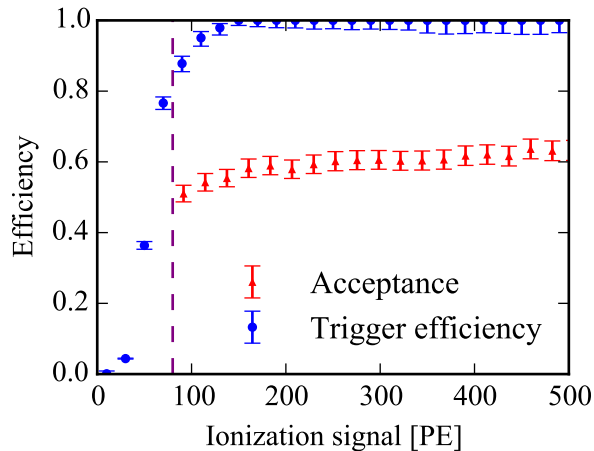
FIG. 3. The analysis acceptance (red triangles) and the trigger efficiency (blue circles). The purple dashed line is the analysis threshold (80 PE).

These are most likely caused by radioactivity from the top PMT array. In these so-called "gas events", a larger than average fraction of the S2 light is seen by the top PMT array since the S2 signal is produced close to it. The S2 signal is also wider than an S2 produced in the liquid since the luminescence region is typically twice as wide and – if an S1 signal is detected – it occurs very shortly before the S2. Therefore, we define an asymmetry parameter $(S2_{top} - S2_{bottom}) / (S2_{top} + S2_{bottom})$, corresponding to the fraction of observed light in the top PMTs compared to the bottom PMTs.

In Fig. 2, the asymmetry parameter is shown for ^{241}AmBe events that occurred in the liquid xenon and a sample of events from interactions in the gas phase. The gas events are selected from ^{60}Co and the DM search data by requiring an S2 width at 10% peak height and a drift time, which is inconsistent with the diffusion broadening expected for a liquid xenon event. Both distributions are normalized to the rate expected in the DM search data. The liquid events should be primarily due to ERs from background γs, so we estimate the rate by comparing the rate of ^{60}Co events and DM search data events at energies far beyond the region of interest, as done in [13]. The gas event rate was estimated from DM search data events with an S2 asymmetry larger than 0.45 (again, well beyond the region of interest), as seen in Fig. 2.

We remove events with an S2 asymmetry parameter larger than 0.17. This threshold is chosen by optimizing the ratio of the liquid events over the square root of gas events. Only 65% of normal S2 signals at 100 PE will pass the asymmetry cut (as determined from the ^{241}AmBe data). The low acceptance is justified because of the gas event background in this analysis.

Figure 3 shows the analysis acceptance as a function of the S2 signal size. The acceptances are estimated using ^{60}Co and ^{241}AmBe, which are similar and agree within a 3% systematic uncertainty. Figure 3 also shows the

measured XENON100 trigger efficiency [13]. The trigger efficiency in our region of interest is more than 80%. The product of the trigger efficiency and analysis acceptance is our final signal detection efficiency. Table I shows the acceptance of the analysis selections discussed above, as well as the number of events remaining at each stage. After applying the data selection cuts summarized in Table I to the the entire dataset of $30\,\mathrm{kg} \times \mathrm{yr}$, 13560 valid candidate events remain in the S2 range $[80, 1000]\,\mathrm{PE}$, see Fig. 4.
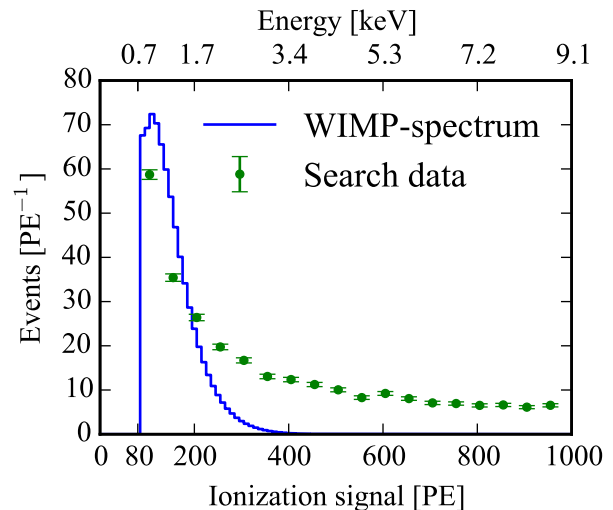

FIG. 4. Energy distribution of the events remaining in the dataset after all data selection cuts. As example, the expected spectrum for a WIMP of $6\,\mathrm{GeV}/c^2$ and a spin-independent WIMP-nucleon scattering cross section of $1.5 \times 10^{-41}\,\mathrm{cm}^2$ is also shown. The corresponding nuclear recoil energy scale is indicated on the top axis. The charge yield model assumed here has a cut-off at $0.7\,\mathrm{keV}$, which truncates the WIMP spectrum.

IV. RESULTS

The interpretation of the outcome of the data selection requires the reconstruction of a nuclear recoil equivalent energy scale from the measured S2 signals. It is based on two quantities: the first one is the charge yield Q_y, shown in Fig. 5, which gives the number of ionization electrons per keV liberated by a NR event. The second one is the secondary scintillation gain Y, which is detector-dependent and gives the number of proportional scintillation photoelectrons per electron extracted into the gas phase. In this science run of XENON100, Y is described by a normal distribution with $\mu = (19.7 \pm 0.3)\,\mathrm{PE/e^-}$ and $\sigma = (6.9 \pm 0.3)\,\mathrm{PE/e^-}$ [12]. Charge extraction from the liquid is almost unity at the XENON100 extraction field [9].

As shown in Fig. 5, where measurements and models differ at the 50% level, there is some remaining uncer-
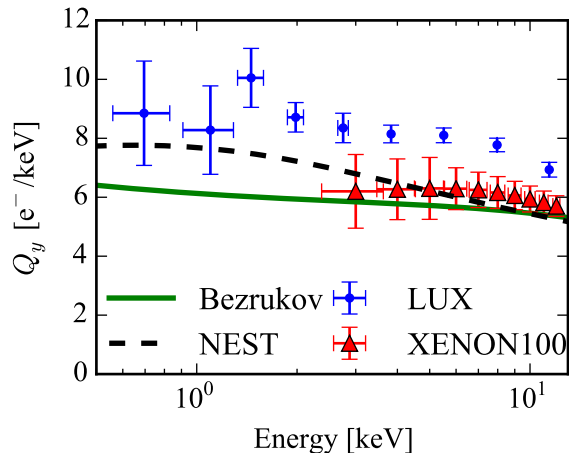
FIG. 5. Charge yield (Q_y) as a function of energy for nuclear recoils (keV). This analysis employs the conservative nuclear recoil charge yield model of Bezrukov et al. (electric field independent) [16], given by the green line. It agrees with the measurement of XENON100 (E = 0.53 kV/cm) [14] (red triangles) while the NEST model (E = 0.73 kV/cm) [17] (dashed black) and the recent measurement of LUX (E = 0.18 kV/cm) [15] (blue points) predict higher yields. To account for the mild discrepancies at low energies, we use the model from Bezrukov et al. and conservatively assume Q_y=0 below 0.7 keV.

FIG. 6. S2 spectrum of ^{241}AmBe calibration data compared to simulations using the Q_y from Bezrukov et al. [16] with no energy cut-off.

FIG. 7. WIMP exclusion limit on the spin-independent WIMP-nucleon scattering cross section at 90% confidence level. Limits from the LUX [15], XENON100 [10], Super-CDMS [21], CDMSlite [22], XENON10 [8], CRESST-II [23] experiments are shown. The claims from DAMA/LIBRA experimental data [24] and CDMS-II (Si detectors) [7] are also shown . The limit from this analysis is shown with the thick blue line and it improves the XENON100 result [10] (dashed blue line) for WIMP masses below $\sim$7.4 GeV/c^2.

tainty in Q_y, especially at very low recoil energies, even though the LUX data demonstrate clearly that Q_y is non-zero above 0.7 keV [15]. In order to not base our WIMP result on optimistic assumptions, we use the analytical model of Bezrukov et al. [16], which agrees with the XENON100 measurement [14] and the NEST model [17] above $\sim$6 keV and is more conservative at lower energies. We additionally introduce a cut off at 0.7 keV, below which Q_y is set to zero, to penalize the result for the limited knowledge on the charge yield at the lowest energies. This energy also corresponds to the threshold at which signals will be above our 80 PE threshold.

However, we note that a Monte Carlo model based on the Bezrukov et al. function without any cutoff leads to a good description of the measured charge-spectrum from ^{241}AmBe calibration data, see Fig. 6. The data were selected based on the same criteria as used in the WIMP analysis, with the exception of the S2 asymmetry cut, which is not required due to the significantly higher rate of the ^{241}AmBe source compared to the gas event rate. Besides the statistical uncertainty, the spectrum also includes a systematic uncertainty of 8%, which is mainly due to the uncertainties in the S2 amplification [12] and the cut acceptance. The simulation follows the strategy described in [14] but ignores the S1 light information.

The same Monte Carlo method is used to model the expected WIMP spectra. The number of electrons released after a nuclear recoil of energy E is given by a Poisson distribution with mean $N = EQ_y$. The charge
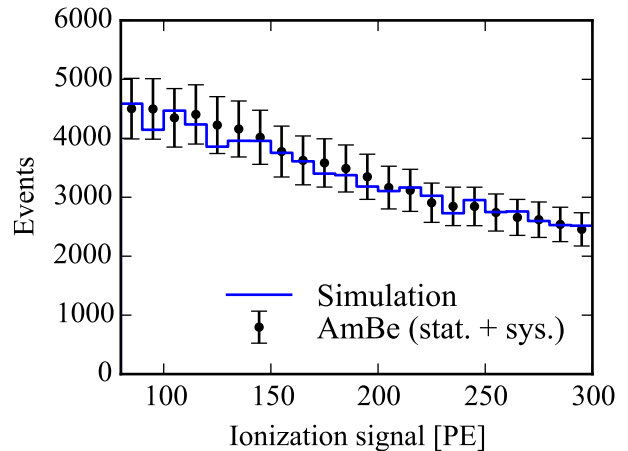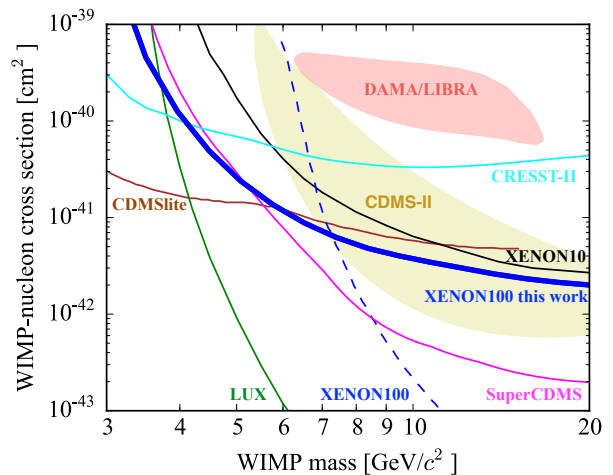
loss due to the finite electron lifetime τ_e is taken into account by using the average $\tau_e = 570\,\mu s$ measured in this run [13]. Since no information on the z-coordinate is available, we correct each event by averaging the exponential survival probability throughout the TPC. The secondary scintillation is modeled using the measured parameters given above and in [12]. A Maxwell-Boltzmann distribution with the asymptotic velocity of the local system $v_0 = 220\,km/s$, the solar velocity $v_{sun} = 232\,km/s$ and the galactic escape velocity $v_{esc} = 544\,km/s$ is used

to model the DM halo, assuming a local WIMP density of $\rho_0 = 0.3\,\mathrm{GeV}/(c^2 \times \mathrm{cm}^3)$ [18]. As an example, Fig. 4 shows the NR spectrum, as parameterized in [19], induced by a $6\,\mathrm{GeV}/c^2$ WIMP at a spin-independent cross section of $\sigma = 1.5 \times 10^{-41}\,\mathrm{cm}^2$. We observe an event rate of ~ 0.5 events/(keV$\times$kg$\times$day) between 0.7 and 1.7 keV that drops to ~ 0.07 events/(keV$\times$kg$\times$day) between 3.4 and 9.1 keV.

In the absence of a full background model, which cannot be constructed as the origin of the small-S2 background in the detector cannot be reliably quantified, we assume that every event passing the analysis cuts could be due to a DM interaction. The analysis employs the optimum interval method [20] and will therefore always lead to an exclusion limit. The low-mass WIMP result for this $30\,\mathrm{kg} \times \mathrm{yr}$ XENON100 exposure is based on all events remaining in the 80-1000 PE interval (0.7-9.1 keV), the NR acceptance of Fig. 3 and is shown in Fig. 7. At a WIMP mass of $6\,\mathrm{GeV}/c^2$, XENON100 excludes spin-independent WIMP-nucleon interaction cross sections of $1.2 \times 10^{-41}\,\mathrm{cm}^2$ at 90% confidence level. The moderate improvement upon the XENON10 low-mass result [8], despite the much larger exposure, is due to the significantly

higher background from photo-ionization events, which is enhanced by the presence of larger metal surfaces inside the TPC. The new result challenges a standard WIMP interpretation of the DAMA/LIBRA modulation signal, excludes large fractions of the CDMS-II (Si) preferred region and improves the result of the previous XENON100 result [10] below $\sim 7.4\,\mathrm{GeV}/c^2$. We improve the LUX [15] (SuperCDMS [21]) results below ~ 3.7 (5.4) GeV/c^2.

V.   ACKNOWLEDGMENTS

[1] P. Ade et al. (Planck collaboration), arXiv:1502.01589.
[2] M. W. Goodman and E. Witten, Phys. Rev. D 31, 3059 (1985).
[3] G. Jungman, M. Kamionkowski, and K. Griest, Phys. Rept. 267, 195 (1996).
[4] D. E. Kaplan, M. A. Luty, and K. M. Zurek, Phys. Rev. D 79, 115016 (2009).
[5] T. Lin, H. Yu, and K. Zurek, Phys. Rev. D 85 (2012) 063503.
[6] R. Bernabei et al. (DAMA/LIBRA collaboration), Eur. Phys. J. C 73, 2648 (2013).
[7] R. Agnese et al. (CDMS-II collaboration), Phys. Rev. Lett. 111, 251301 (2013).
[8] J. Angle et al. (XENON10 collaboration), Phys. Rev. Lett. 107, 051301 (2011).
[9] E. Aprile et al. (XENON100 collaboration), Astropart. Phys. 35, 573-590 (2012).
[10] E. Aprile et al. (XENON100 collaboration), Phys. Rev. Lett. 109, 181301 (2012).
[11] E. Aprile et al. (XENON100 collaboration), Phys. Rev. Lett. 111, 021301 (2013).
[12] E. Aprile et al. (XENON100 collaboration), J. Phys. G: Nucl. Part. Phys. 41, 035201 (2014).
[13] E. Aprile et al. (XENON100 collaboration), Astropart. Phys. 54, 11-24 (2014).
[14] E. Aprile et al. (XENON100 collaboration), Phys. Rev. D 88, 012006 (2013).
[15] D. S. Akerib et al. (LUX collaboration), Phys. Rev. Lett. 116, 161301 (2016).
[16] F. Bezrukov, F. Kahlhoefer, M. Lindner, Astropart. Phys. 35, 119-127 (2011).
[17] B. Lenardo et al., IEEE Trans. on Nucl. Sci. vol.62, 3387-3396 (2015).
[18] A. M. Green, Mod. Phys. Lett. A27 1230004 (2012).
[19] J.D. Lewin, P.F. Smith, Astropart. Phys. 6 87-112 (1996).
[20] S. Yellin, Phys. Rev. D 66, 032005 (2002).
[21] R. Agnese et al. (SuperCDMS collaboration), Phys. Rev. Lett. 112, 241302 (2014).
[22] R. Agnese et al. (SuperCDMS collaboration), arXiv:1509.02448.
[23] G. Angloher et al. (CRESST collaboration), arXiv:1509.01515v1.
[24] C. Savage, G. Gelmini, P. Gondolo and K. Freese, JCAP no. 04 010 (2009).